Cell, Vol. 87, 297–306, October 18, 1996, Copyright ©1996 by Cell Press

Structure of the C-Terminal Region of p21$^{WAF1/CIP1}$ Complexed with Human PCNA

Jacqueline M. Gulbis,* Zvi Kelman,‡# Jerard Hurwitz,‖ Mike O'Donnell,‡§ and John Kuriyan*†
*Laboratory of Molecular Biophysics
†Howard Hughes Medical Institute
The Rockefeller University
New York, New York 10021
‡Department of Microbiology
§Howard Hughes Medical Institute
Cornell Medical College
New York, New York 10021
‖Program in Molecular Biology
Memorial Sloan-Kettering Cancer Center
1275 York Avenue
New York, New York 10021

Summary

The crystal structure of the human DNA polymerase δ processivity factor PCNA (proliferating cell nuclear antigen) complexed with a 22 residue peptide derived from the C-terminus of the cell-cycle checkpoint protein p21$^{WAF1/CIP1}$ has been determined at 2.6 Å resolution. p21 binds to PCNA in a 1:1 stoichiometry with an extensive array of interactions that include the formation of a β sheet with the interdomain connector loop of PCNA. An intact trimeric ring is maintained in the structure of the p21–PCNA complex, with a central hole available for DNA interaction. The ability of p21 to inhibit the action of PCNA is therefore likely to be due to its masking of elements on PCNA that are required for the binding of other components of the polymerase assembly.

Introduction

The arrest of DNA replication in response to the detection of DNA damage is a fundamental mechanism by which the cell minimizes the potential transmission of lethal mutations. One mediator of this response is the protein p21$^{WAF1/CIP1}$ (hereafter referred to as p21), an inhibitor of the cyclin-dependent protein kinases (cdks) that control the initiation of the S phase of the cell cycle and concomitant DNA replication (El-Deiry et al., 1993; Gu et al., 1993; Harper et al., 1993; Noda et al., 1994; for review see Peter and Herskowitz, 1994). An elevation of nuclear levels of the tumor suppressor protein p53 occurs upon detection of DNA damage. This stimulates transcription of p21 as part of a p53 signaling pathway in which the cessation of DNA replication is coupled to stalling of cellular mitosis (Waldman et al., 1996). In addition, the levels of p21 also respond to certain stimuli, such as growth factors, in a p53-independent manner.

p21 is a member of a family of cdk-inhibitory proteins, including p27^{Kip1} (Polyak et al., 1994), p57^{Kip2} (Lee et al., 1995), and p27^{XIC1} (Su et al., 1995), which share sequence similarity in their N-terminal regions. These highly conserved regions are by themselves sufficient to inhibit cyclin–cdks that function at major transition points in the cell cycle. The structure of the N-terminal region of p27^{Kip1} bound to the cyclin A–Cdk2 complex has been reported recently (Russo et al., 1996). The inhibitor molecule is poorly structured when not bound to cyclin–cdk. The cyclin A–Cdk2 complex acts as a template or scaffolding that induces an extended structure in the 69 residues at the N-terminus of p27^{Kip1}, which binds tightly across the cyclin–cdk interface and the ATP-binding lobe of the kinase. Given the similarity in their N-terminal regions, this structure of the p27^{Kip1}–cyclin A–Cdk2 complex provides a good model for understanding the interactions of p21 with cyclin–cdk complexes (Russo et al., 1996).

However, in contrast to p27^{Kip1} or p57^{Kip2}, p21 is also able directly to inhibit DNA replication by binding tightly to and blocking the action of the DNA polymerase processivity factor PCNA (proliferating cell nuclear antigen; Flores-Rozas et al., 1994; Waga et al., 1994). PCNA is a DNA-tracking protein that is required for the rapid and processive replication of DNA by the polymerases δ and ε because it forms a sliding clamp that tethers the polymerase to DNA during strand synthesis (Kelman and O'Donnell, 1995; Krishna et al., 1994). The C-terminal region of p21$^{WAF1/CIP1}$ is distinct from that in p27^{Kip1} and p57^{Kip2} and contains a PCNA–binding sequence (Warbrick et al., 1995). The overexpression in mammalian cells of C-terminal fragments containing this region is sufficient to arrest DNA replication (Chen et al., 1995b; Goubin and Ducommun, 1995; Luo et al., 1995; Warbrick et al., 1995). Biochemical experiments have shown that this inhibition is due to a direct interaction between p21 and PCNA and that the inhibition can be relieved by excess PCNA (Flores-Rozas et al., 1994; Shivji et al., 1994; Waga et al., 1994). The inhibition of cyclin–cdk by p21 appears to be more critical for the regulation of the G1-to-S transition, and the particular role of the p21–PCNA interaction remains to be determined (Nakanishi et al., 1995). The molar ratio of p21 to PCNA in normal human diploid fibroblasts has been shown to be close to 1:1, suggesting that a direct inhibitory interaction between these two proteins is likely to be biologically relevant (Li et al., 1996). PCNA is also required for nucleotide excision repair (Nichols and Sancar, 1992; Shivji et al., 1992), but the precise effect of p21 on this process also needs further clarification (Li et al., 1994, 1996; Pan et al., 1995; Shivji et al., 1994).

The PCNA–binding functionality of p21 appears to reside entirely in the C-terminal 22 residues of the protein, which also suffice to block PCNA–mediated DNA replication directly (Chen et al., 1996; Pan et al., 1995; Warbrick et al., 1995). A peptide corresponding to these 22 residues binds to human PCNA with high affinity, comparable with that of the intact p21 protein (K_d of approximately 2.5 nM, as measured by biosensor analysis) and efficiently inhibits DNA synthesis in vitro (Gibbs et al., submitted; Pan et al., 1995). The finding that a

Present address: Department of Molecular Biology and Genetics, Johns Hopkins University, Baltimore, Maryland 21205.

relatively short peptide can capture the binding and inhibitory capacity of the p21 protein is particularly intriguing since the architecture of PCNA is not immediately suggestive of a peptide-binding function. The crystal structure of Saccharomyces cerevisiae PCNA (scPCNA) has been determined (Krishna et al., 1994), revealing a ring-shaped molecule that encircles DNA, with no prominent crevices or grooves suggestive of high affinity binding sites for a peptide.

The loading of PCNA onto DNA by the RF–C complex does not appear to be affected appreciably by p21 (Gibbs et al., submitted; Podust et al., 1995). Likewise, the ability of PCNA to move along DNA is also not affected by p21 (Podust et al., 1995). Consequently, p21 is likely to interfere with PCNA–dependent DNA replication by disruption of the structure of PCNA or by preventing attachment of DNA polymerases δ or ϵ to the PCNA ring.

We now report the crystal structure of human PCNA complexed with a peptide corresponding to the 22 C-terminal residues of p21, determined at a resolution of 2.6 Å. The structure reveals that the peptide is anchored on PCNA via hydrogen-bonding interactions that exploit a characteristic feature of the PCNA architecture, a long interdomain connector chain that crosses back over the outer surface of each of the three PCNA molecules in the trimer. In addition to the formation of an antiparallel β strand structure with the connector, basic regions of the p21 peptide complement electrostatically the markedly negative electrostatic potential of the surface of PCNA, and hydrophobic residues in two regions of the peptide are accommodated by hydrophobic cavities on the surface of PCNA that are likely induced by peptide binding. Comparison with the structure of uncomplexed scPCNA reveals that the peptide does not interfere with oligomerization or with the central cavity through which DNA is threaded.

The p21–PCNA interface has the hallmarks of a tight and specific molecular interaction, and by its ability to block DNA replication it maps regions of the PCNA surface that are likely to be important for polymerase attachment. These regions on PCNA are also potential targets for the design of small molecule analogs that might mimic the action of the p21 peptide.

Results and Discussion

Structure Determination

Trigonal crystals of the human PCNA–p21 peptide complex ($P3_221$, a = 83.5 Å, c = 233.9 Å) diffract X-rays beyond 2.6 Å when cryogenically cooled. However, collection of data to this resolution on a conventional laboratory X-ray source is problematic because of the long lattice spacing along the c axis; a dataset complete to 2.6 Å was collected at Brookhaven National Synchrotron Light Source (Beamline X25). The crystal structure was determined by molecular replacement, using the structure of scPCNA as the initial model (Krishna et al., 1994). A well-defined and continuous segment of electron density running alongside the connector loop of PCNA indicated the location of the p21-peptide in initial electron density maps. Of the 22 residues of the peptide (^{139}GRKRRQTSMTDFYHSKRRLIFS^{160}, p21 sequence numbering), 17 are modeled unambiguously. The first five residues at the peptide N-terminus are not clearly visible in the electron density maps and are located in the vicinity of the C-terminal region of PCNA, which is also disordered. A set of two short loops near the intermonomer interface of PCNA is also disordered. The final model of 6,154 nonhydrogen protein atoms and 295 water molecules was refined to values of 28.9% and 19.2% for the free and working R values, respectively, using X-ray data between 7.0 and 2.6 Å. Crystals of human PCNA obtained in the absence of the peptide diffract poorly, and thus no structure of the uncomplexed form was obtained.

Structure of Human PCNA

Human PCNA shares 35% sequence identity with scPCNA (Almendral et al., 1987; Bauer and Burgers, 1990), and its three-dimensional structure is highly similar to the structure of the latter (Krishna et al., 1994; Figure 1). A set of three molecules of PCNA, each consisting of two similar domains, is assembled into a circular ring with a central hole wide enough easily to encircle duplex DNA (Figure 2). The structures of human and yeast PCNA are closely superimposable over the core secondary structural elements, with a root-mean-square deviation of 0.9 Å for 170 C^{α} positions in the monomers (Figure 1b). Each of the secondary structural elements of scPCNA is preserved in human PCNA (for notation see Figure 1). Antiparallel interactions between strands βD_2 and βI_1 in adjacent PCNA subunits are the key elements in the intermolecular interface and lead to the formation of a total of three nine-stranded β sheets that form a contiguous surface across each intermolecular boundary. Likewise, antiparallel interactions between strands βD_1 and βI_2 within one molecule result in the formation of three similar β sheets across the interdomain boundaries within one molecule. Together, these six curved β sheets form an outer scaffold that supports an inner lining of 12 α helices that are oriented approximately perpendicular to the ring face.

The PCNA ring has a distinct front and back. On one face, a number of prominent loops connecting adjacent antiparallel β strands protrude into solvent (in particular βD_2–βE_2 and βH_1–βI_1), while on the other a long loop (βI_1–βA_2, the interdomain connector loop) links the N- and C-terminal domains of each monomer. In terms of topological elements, this connector loop provides the most obvious deviation from pseudohexagonal symmetry, as it traverses the intrasubunit but not intersubunit domain boundaries.

The Protein–Peptide Interface

A 22 residue peptide is bound to each of the three PCNA subunits of the ring (Figures 1 and 2). Binding of the p21 peptide to PCNA involves an extensive set of interactions spanning the entire length of the peptide and burying 2,242 Å^2 of total surface area at the intermolecular interface (57% on the peptide, 43% on PCNA). The peptide inhibitor binds in an almost fully extended conformation across one face of each PCNA subunit, leaving the hole in the middle of the ring uncovered (Figure 2).

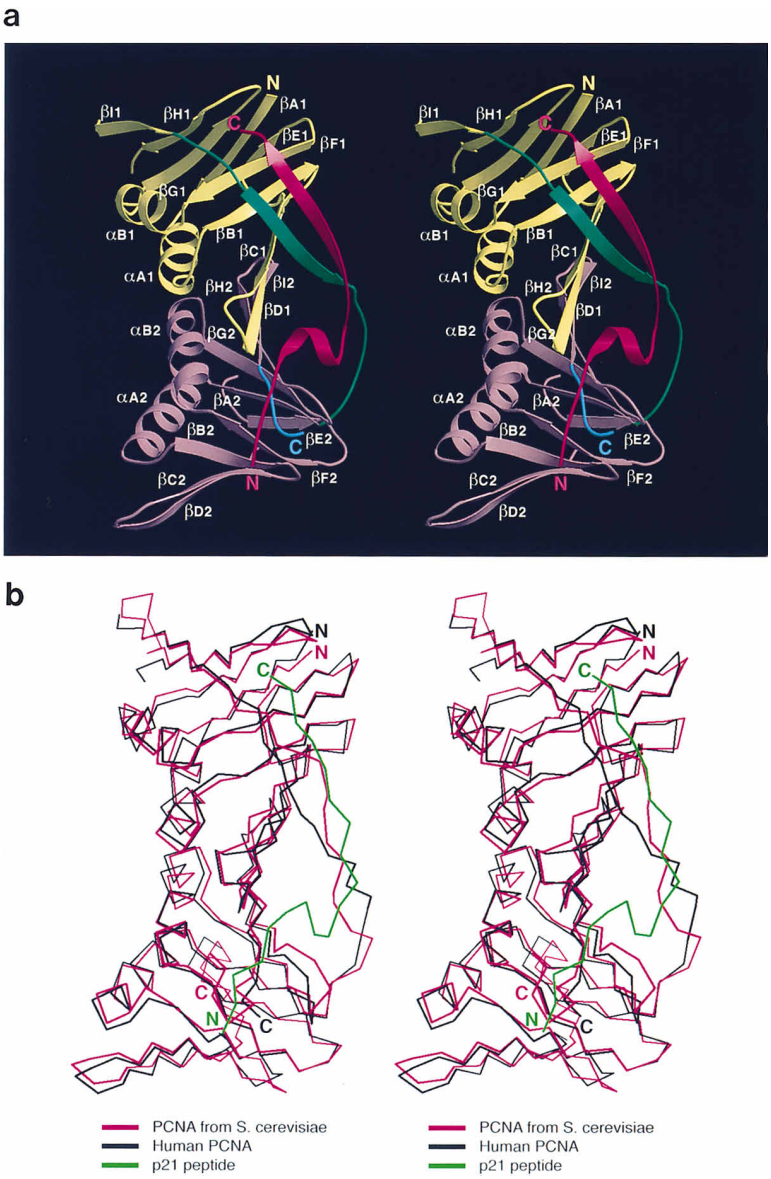

Figure 1. Ribbon Diagram of the PCNA Monomer with Bound p21 Peptide

(a) Stereo diagram of the three-dimensional structure of one monomer of the PCNA–p21 peptide complex, looking directly onto the face of the ring. The peptide (colored red) runs alongside the interdomain connecting loop (green). The N-terminal domain of PCNA is drawn in yellow and the C-terminal domain in plum, with five residues at the terminus shaded blue. Figure prepared using the programs MOLSCRIPT (Kraulis, 1991) and Raster-3D (Bacon and Anderson, 1988).

(b) Superimposition of the C^{α} trace of PCNA from S. cerevisiae (red) onto that of human PCNA (black) with bound p21 peptide (green). The orientation is similar to that in (a). Prepared using the programs O (Jones et al., 1991) and MOLSCRIPT (Kraulis, 1991).

It has been reported that p21 might destabilize the PCNA trimer, as assayed by glutaraldehyde cross-linking and Western blot analysis (Chen et al., 1995a). In structural terms, the peptide does not interfere directly with oligomerization of PCNA; each peptide contacts only one subunit and does not overlap the intermolecular interface. Destabilization of the PCNA trimer is therefore not likely to be a major mechanism for p21 action.

The peptide makes contacts with three distinct regions of the PCNA surface, resulting in interactions with residues from both domains and the interdomain connector. The C-terminal region of the peptide forms an antiparallel β sheet with the connector loop of PCNA, resulting in seven interprotein backbone amide-to-carbonyl hydrogen bonds. The side chains of the peptide in this region interact with residues from the N-terminal domain of PCNA that lie under the interdomain connector. Secondly, three central residues of the peptide are anchored in a hydrophobic cleft between the connector loop, loops βC_1–βD_1 and βG_2–βH_2, and the C-terminus of PCNA. Finally, residues from the N-terminal portion of the peptide interact with the C-terminus of the PCNA molecule. The residues involved in the third interaction are poorly ordered (GRKRR in p21 and IEDEEGS at the C-terminus of PCNA). However, the relative positions of the residues in the structure make it clear that ion-pairing interactions occur and that the disorder in the structure probably arises from the multiple possibilities for such interactions.

Interactions between the Peptide and the Interdomain Connector

The nine C-terminal residues of the peptide (^{152}HSK RRLIFS^{160}) form a β strand that runs antiparallel to one formed by the N-terminal portion of the interdomain connector loop (see Figure 1). Ion-pairing and hydrogen-bonding interactions are formed between Arg-155 and Arg-156 of the peptide and PCNA residues Glu-124 and

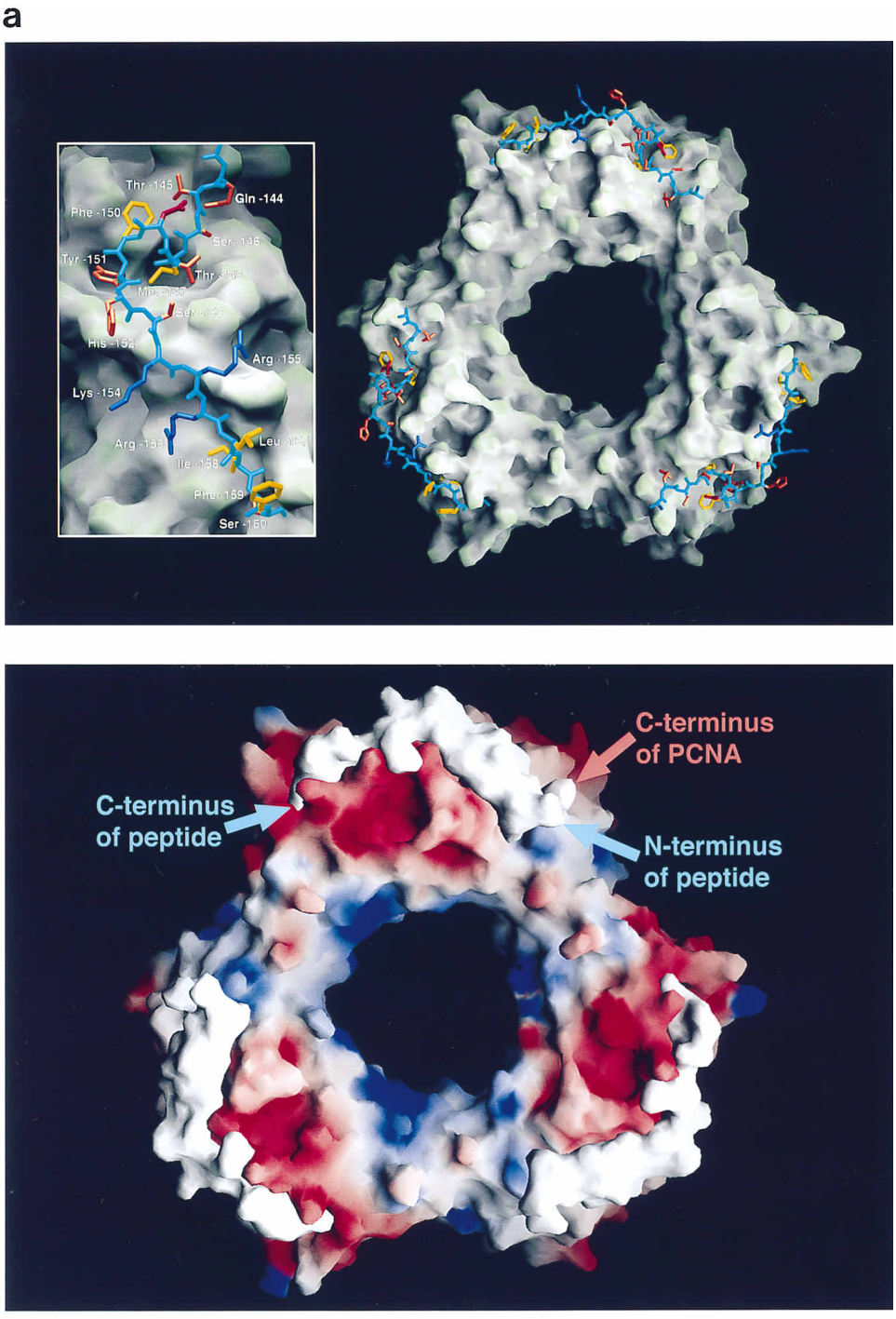

Figure 2. Solvent-Accessible Surface of the PCNA Trimer

(a) The peptide is shown as a stick representation, with side chains colored according to their physical properties (negatively charged residues are drawn in red, positively charged in blue, polar in orange, and hydrophobic in yellow). An enlarged view of the peptide-binding surface is shown in the inset. This figure was generated using GRASP (Nicholls et al., 1991).

(b) Molecular surface of the complex, with PCNA colored according to electrostatic potential and the peptide shown in white. In the calculation of electrostatic potential, we used dielectric constants of 2.0 for the protein interior and 80 for solvent at an ionic strength equivalent to 100 mM KCl. Side chains of lysine and arginine residues were given a net positive charge and aspartate and glutamate negative, with other residues considered neutral. Regions of intense positive charge appear blue, and electronegative regions of the surface are red.

Gln-125 from the connector loop, and Asp-29 from strand βB_1. A small hydrophobic pocket formed at the junction of the connector loop and the underlying β sheet of the N-terminal domain of PCNA accommodates the side chain of Ile-158 of the peptide. The hydroxyl of Ser-160 of the peptide participates in two hydrogen bonds to the PCNA backbone. Ser-160 also interacts via the main-chain nitrogen with the carboxylate of Asp-120 (Figure 3a).

The observed interaction between the p21 peptide and the interdomain connector is consistent with the results of Warbrick et al. (1995), who showed that the connector region of PCNA is necessary for p21 binding. The sequence of nine residues (^{152}HSKRRLIFS^{160}) is important for the inhibition of DNA replication by p21; related peptides from the C-terminus of p21 that do not include this segment lack the capacity to block replication (Warbrick et al., 1995). Results of alanine scan mutations reported in that study are also consistent with the structure of the p21–PCNA complex. Truncation to C^{β} of the side chains of Arg-155, Arg-156, Ile-158, or Ser-160 (mentioned earlier as interacting with PCNA residues) decreased inhibitory activity of the peptide, whereas truncating the side chains of His-152, Ser-153, Leu-157, or Phe-159, which make no polar or hydrophobic contacts with PCNA, does not appear to affect the biological activity significantly (Warbrick et al., 1995).

The connector loop of PCNA is an architectural feature of particular interest on the exterior of an otherwise symmetrical molecule. It arises as a consequence of the modular construction of the PCNA ring, in which each subunit comprises two topologically similar domains that are linked in a head-to-tail fashion but where the arrangement of secondary structural elements is such that the terminal strand of the first domain does not abut the first strand of the second but is located approximately 40 Å away. This necessitates a very long crossover loop to connect the two domains (see Figure 1). As it traverses the interdomain boundary, this polypeptide chain (PCNA residues 119–134) is involved in a number of interactions with residues from the surface of the underlying β sheet, but the hydrogen-bonding potential of the backbone of the connector loop is not utilized and is available for interaction with other molecules such as p21.

Hydrophobic Interactions

The eight–amino acid motif (^{144}QTSMTDFY^{151}) in the central part of the p21 peptide is required for binding to PCNA; in particular, Met-147 and Phe-150 of p21 are critical for recognition of PCNA (Nakanishi et al., 1995; Warbrick et al., 1995). In the structure of the complex, residues (^{146}SMTDFY^{151}) adopt a 3_{10} helical conformation, stabilized by an intramolecular hydrogen-bonding network in which the carboxyl moiety of Asp-149 accepts hydrogen bonds from both the amide nitrogen atom of Thr-145 and the side-chain hydroxyl of Ser-146, while the O^{γ} of Thr-148 of p21 interacts with the hydroxyl of this same serine residue. This configuration positions both Met-147 and Tyr-151 of p21 in a hydrophobic cavity under the connector loop of PCNA. The Phe-150 side chain of the peptide does not enter this cleft but rather provides a boundary to the exterior and is itself packed against two proline residues (Pro-234 and Pro-253; Figure 3). The hydroxyl group of Tyr-151 forms a hydrogen bond with Gln-131 of PCNA and additionally, via an ordered water molecule, interacts with the hydroxyl of Tyr-133 and the backbone carbonyl of Pro-234 (Figure 3a). The polar side chains of Gln-144 and Thr-145 of the peptide form hydrogen bonds with the main-chain carbonyls of Ala-252 and Pro-253 at the C-terminus of PCNA. A well-ordered water molecule bridges between the O^{ϵ} of the glutamine and the amide-nitrogen atom of Ala-208 at the C-terminal end of the βF_2 strand of PCNA.

The hydrophobic crevice in human PCNA that binds to Met-147 and Tyr-151 of the p21 peptide is not apparent in the structure of scPCNA and is formed by a shift in the position of the interdomain connector loop (see Figure 1b). This conformational change in human PCNA may have been induced by peptide binding, since the structures of human and S. cerevisiae PCNA overlap closely in all other regions (see Figure 1b). However, the amino acids in the connector loop are divergent in sequence (only 15% sequence identity), and in the absence of a structure for the uncomplexed form of human PCNA, the origin of the structural difference is unclear. It is interesting to note that despite the close overall structural similarity between the two PCNAs, the p21 peptide does not bind to scPCNA and is unable to inhibit DNA replication carried out by S. cerevisiae Pol δ, RF–C, and scPCNA (Gibbs et al., submitted). This difference in binding ability can be explained by sequence differences in the interdomain connector and adjacent regions of the two PCNA molecules (Gibbs et al., submitted).

Electrostatic Complementarity between the p21 Peptide and PCNA

Calculation of the electrostatic potential of human PCNA shows that the surface of the trimer has a highly negative potential, except in the central channel where a region of positive potential is created by several lysine and arginine side chains (see Figure 2b). This is true of all known structures of sliding clamps, and the positive charge in the central region is thought to be important in stabilizing the PCNA trimer on the negatively charged phosphate backbone of DNA (Fukuda et al., 1995; Krishna et al., 1994). It has been noted that the C-terminal region of p21 contains a classical bipartite nuclear localization signal, in which two basic regions are separated by about 10 residues, some of which are hydrophobic (El-Deiry et al., 1993; Robbins et al., 1991). The two basic regions of the peptide complement electrostatically the negatively charged surface of PCNA. A total of seven positively charged groups on each peptide interact with a similar number of negatively charged groups on each monomer of PCNA, including the carboxyl group at the C-terminus.

The N-terminal basic residues of the peptide (^{139}GR KRR^{143}) are not visualized in the electron density maps, but it appears that they interact with the highly acidic C-terminal tail of PCNA (^{256}EDEEGS^{261}). Residues Lys-254 and Ile-255 of PCNA and residues Arg-143, Gln-144, and Thr-145 of p21 are arrayed antiparallel to each

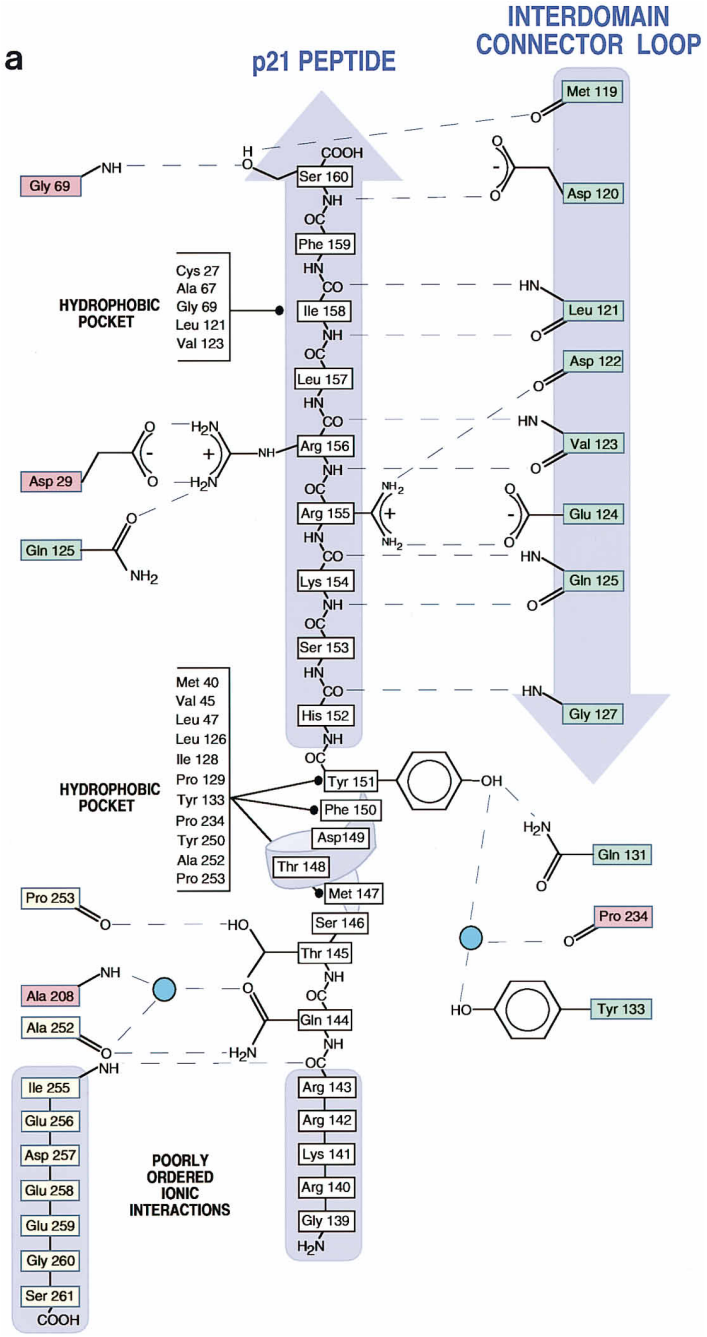

Figure 3. Interactions at the p21–PCNA Interface

(a) Schematic depiction of contacts between the peptide and PCNA. Residues of the connector loop of PCNA are shaded green, those of the C-terminus are in yellow, and other PCNA residues are in pink. A set of two water-mediated contacts is also shown (blue circles).

(b) Hydrophobic interactions at the p21–PCNA interface. A set of four side chains of the p21-peptide (red) fit into hydrophobic cavities in the molecular surface of PCNA. The C^{α} trace of PCNA is displayed as a green tube. PCNA residues lining the pockets (shown in yellow) are: Cys-27, Met-40, Val-45, Leu-47, Ala-67, Gly-69, Leu-121, Val-123, Leu-126, Ile-128, Pro-129, 133-Tyr, Pro-234, Tyr-250, Ala-252, Pro-253, and (in green) Gln-131, which contacts the hydroxyl of the peptide tyrosine. This figure was generated using GRASP.

(*Figure 3 continued on next page*)

other. Although the model cannot be extended beyond these residues unambiguously, the spatial disposition of the two peptide chains suggests that the remaining four N-terminal residues of p21 and the six C-terminal residues of PCNA are associated closely.

Conclusion

High processivity during chromosomal replication is facilitated by the attachment of the catalytic subunits (DNA polymerase and exonuclease) to a sliding-clamp protein that encircles the DNA, enabling the polymerase

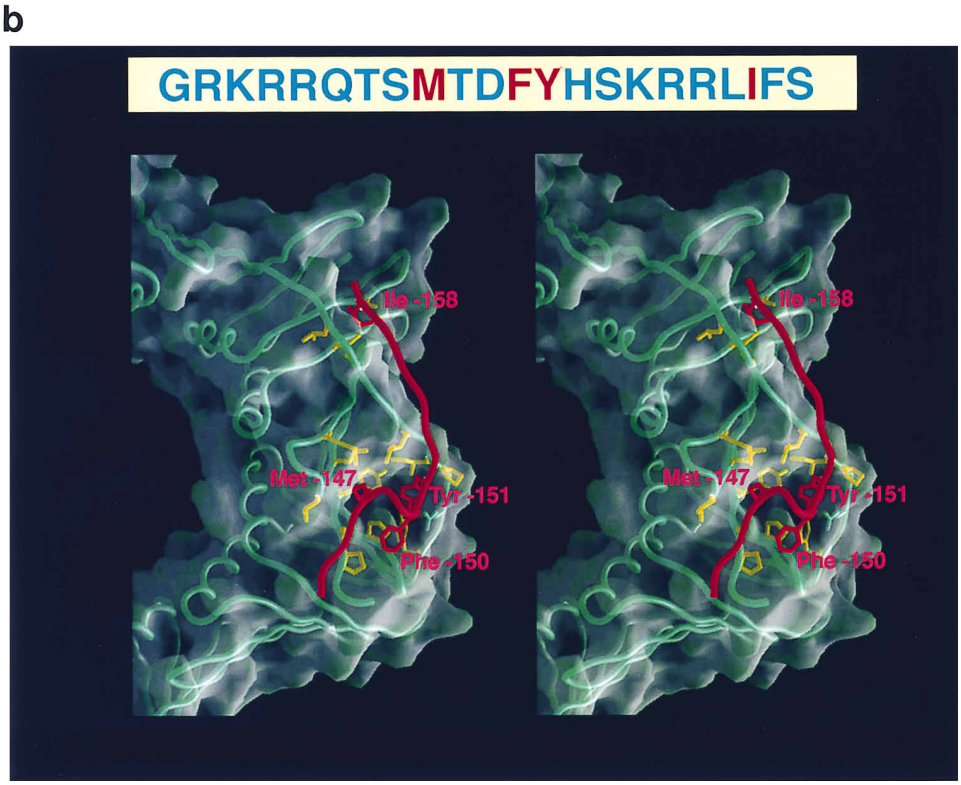

to move rapidly along DNA without dissociation from the template. The close similarity in the architectures of PCNA and the β subunit of Escherichia coli DNA polymerase III showed that this basic mechanism of processive DNA replication was conserved between prokaryotic and eukaryotic systems (Kong et al., 1992; Krishna et al., 1994). Recent evidence indicates that p21 blocks PCNA–dependent DNA replication by preventing chain elongation rather than by affecting RFC–catalyzed clamp loading (Gibbs et al., submitted; Podust et al., 1995). The structure of the inactive p21–PCNA complex shows that p21 binds tightly but with minimal perturbation to the PCNA structure. The major elements of PCNA that are engaged by the p21 peptide (the interdomain connector and the C-terminal tail) are conserved, in architectural terms, in the E. coli β subunit structure. This suggests that the p21–PCNA interaction represents the jamming of an interfacial region that is fundamental to the interaction with the polymerase subunit. Consistent with this, an antibody whose epitope spans the connector loop of human PCNA (residues 121–135) efficiently inhibits DNA replication in vitro (Roos et al., 1996). Mutation of Asp-122 to Ala in the connector loop of human PCNA affects Pol δ stimulation by PCNA but not the interaction with RF–C (Fukuda et al., 1995).

In addition to the interaction with p21 described here, PCNA has been shown to interact directly with cyclin D (Matsuoka et al., 1994) and with the cell cycle–dependent protein Gadd45 that is also induced by DNA damage (Smith et al., 1994). In both cases, mapping of the interaction region by deletion mutagenesis indicates that the interface with PCNA is extensive, including residues from both domains of PCNA (Chen et al., 1995a; Hall et al., 1995; Matsuoka et al., 1994). A more detailed comparison with the binding mode of p21 is not yet possible because of a lack of sequence similarity between these proteins and owing to the coarse resolution of the deletion analysis.

Comparison of the structure of the p21–PCNA complex with that of the $p27^{Kip1}$–cyclin–cdk complex (Russo et al., 1996) shows that p21 will be able to bind both its targets simultaneously, consistent with the observation that in normal eukaryotic cells PCNA is found in complex with cyclin–cdk and p21 (Xiong et al., 1993). The region of p21 that interacts with PCNA has been shown to be unstructured in isolation (Chen et al., 1996), as has the region of $p27^{Kip1}$ that binds to cyclin–cdk (Russo et al., 1996). The p21 inhibitor can therefore be thought of as a molecular grappling hook that has flexible and extensible ends which become structured and tightly attached upon recognition of the proper targets.

Experimental Procedures

Crystallographic Data

Recombinant human PCNA (Almendral et al., 1987) was expressed in E. coli and purified as described previously (Kelman, 1996). Briefly, E. coli strain BL21 (DE3) pLysS was used to express human PCNA, which was purified by standard methodologies, using chromatography on Q Sepharose Fast Flow and Heparin Sepharose (Pharmacia). The protein was extensively dialyzed against 20 mM Tris–HCl (pH 7.5), 2 mM dithiothreitol, 0.5 mM EDTA, and 10% glycerol (no salt) and concentrated. A 1.5-fold molar excess of synthetic p21 peptide (^{139}GRKRRQTSMTDFYHSKRRLIFS^{160}) was incubated with human PCNA (20 mg/ml). The complex that formed was used to screen for crystallization conditions using the hanging-drop vapor diffusion method and revealed a number of conditions for crystal growth. Of

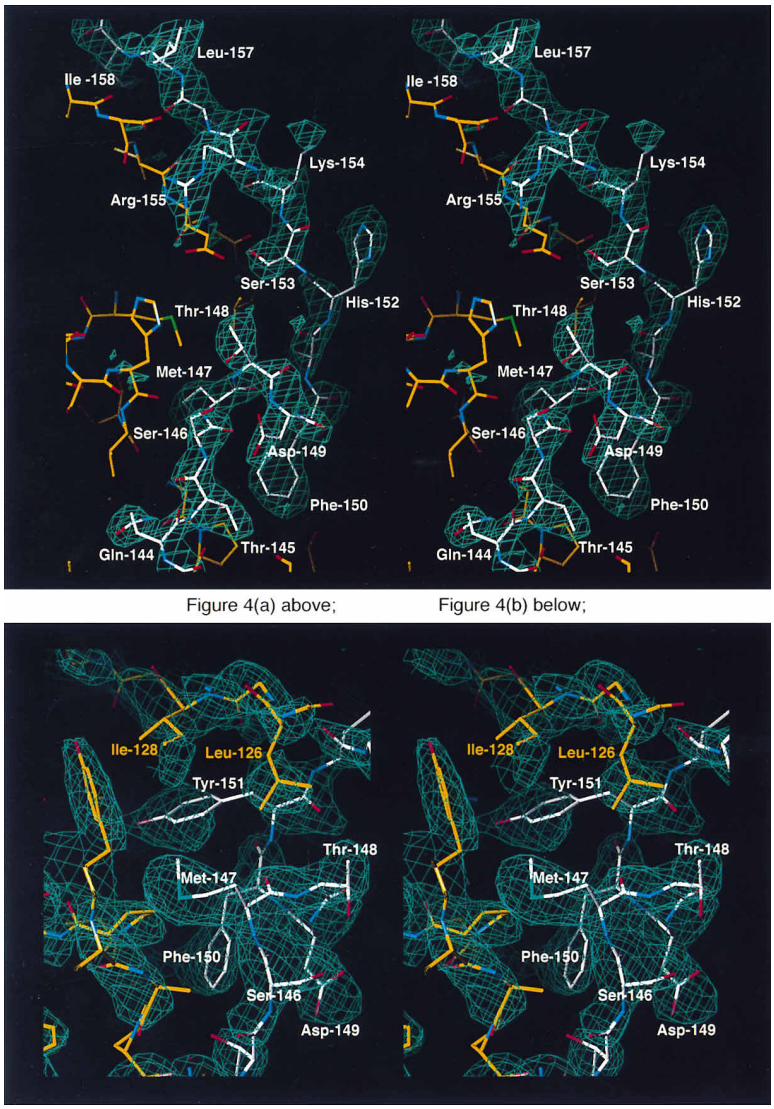

Figure 4(a) above; Figure 4(b) below;

Figure 4. p21 Peptide Binding Site on PCNA

(a) Difference electron density for the p21-peptide. To calculate the electron density map, we deleted residues of one peptide and subjected the remaining atoms to refinement using a simulated annealing protocol (Brünger et al., 1990). The resulting coordinates were used to generate structure factor amplitudes and phases for a Fourier synthesis. The peptide is shown with the carbon atoms colored white.

(b) Electron density for the peptide and PCNA connector loop is clearly evident in a 3-fold averaged 2|Fo|-|Fc| map (15.0–3.0 Å; contoured at 1.5 σ) calculated from the molecular replacement solution prior to any rebuilding or positional refinement of the model.

these, two crystal forms diffracted X-rays strongly enough to enable data collection.

To obtain crystal form I, 1 μl of the complex was mixed with 0.5 μl of 1 M spermine and 1 μl of a reservoir solution containing 100 mM sodium citrate (pH 5.6), 30% (v/v) 2,5-methylpentanediol (MPD), and 200 mM sodium/potassium phosphate. Crystals grown at 4°C under these conditions are trigonal (point group 32, a = 83.5 Å, c = 233.9 Å) with one PCNA trimer in the asymmetric unit and diffract to around 2.6 Å on a conventional X-ray source.

Crystal form II grows at 4°C from 100 mM MES (pH 6.0), 30% (v/v) MPD, and 200 mM magnesium acetate (space group P3; a = 143.2 Å, c = 41.4 Å). Although this crystal form diffracts X-rays strongly to Bragg spacings of 2.0 Å, it is characterized by perfect hemihedral twinning, and diffraction from the crystals is consistent with the Laue group 6/m. Using this crystal form, a model for PCNA and part of the peptide was built based on a molecular replacement solution in which scPCNA was utilized as a search model; the data were detwinned according to the procedure of Redinbo and Yeates (1993). Refinement of this model proved unsatisfactory and was not pursued. Structure determination therefore proceeded using crystal form I.

Crystals of form I were initially transferred into reservoir solution containing an increased concentration of MPD (35%). They were then mounted in nylon loops with the longest cell axis approximately colinear with the spindle and flash-frozen at 100 K. Data to 2.6 Å resolution were collected from a single crystal using a 30 cm MAR imaging plate system on Beamline X25 at Brookhaven National Synchrotron Light Source. All images were processed using the program DENZO, and the integrated intensities were scaled and merged with SCALEPACK (Z. Otwinowski and W. Minor, unpublished data). A set of 130,418 structure factors (33,552 unique) were measured in the resolution range 15.0–2.6 Å, resulting in a dataset that is 96% complete (96.4% in the outer shell). The overall agreement factor, R_{merge} (on intensity), is 7.3% (27.8% in the outer shell).

Structure Solution and Refinement

The PCNA structure was solved by the molecular replacement method using XPLOR (Brünger, 1992). A partially refined model of the human PCNA monomer previously derived from Form II crystals was used to initiate rotation and translation searches in the resolution range 8.0–4.0 Å. A peak 6.7 σ above the mean was the highest in the rotation function. Translation searches using the entire PCNA trimer to enhance signal were calculated in the enantiomorphic space groups $P3_221$ and $p3_121$, in each case finding a peak well above the mean (9.6 σ and 9.4 σ, respectively). A set of 30 cycles of rigid-body refinement of the positioned trimer reduced the R value to 40% in both space groups, using data between 8.0 and 4.0 Å. The distinction between the two space groups is subtle, since the noncrystallographic 3-fold symmetry of each PCNA ring in combination with the 3-fold crystallographic screw-axes results in very similar molecular packing in either case. Refinement proceeded satisfactorily to completion in $P3_221$. Merohedral twinning as seen in

form II crystals was ruled out in this case on the basis of intensity statistics (Redinbo and Yeates, 1993) and by the presence of strong electron density for the peptide in positions related by a 3-fold axis of symmetry (in the twinned crystal form, weak density corresponding to the peptide appears on a physically meaningless 6-fold axis).

For the refinement of the structure, all temperature factors were fixed at 20 Å^2, and the entire connector loop and several residues in other more mobile loops of PCNA were deleted from the starting model. A random 10% of reflections were reserved for a free R value calculation and omitted from refinement procedures. A set of 50 cycles of positional refinement of the PCNA monomer was carried out applying strict noncrystallographic symmetry constraints and using data between 15.0 and 3.0 Å. Electron density maps were then calculated and improved by 3-fold symmetry averaging, using the program suite RAVE (Klewegt and Jones, 1994). The resulting averaged 2Fo-Fc and 3Fo-2Fc Fourier maps were of sufficiently high quality to trace confidently the connecting loop and all but four residues of the peptide using the program O (Jones et al., 1991; Figure 4). Further refinement of the model by least-squares optimization and simulated annealing was carried out using XPLOR (Brünger, 1992). Strict noncrystallographic symmetry constraints were maintained until the final stages.

An anisotropic B-factor tensor was applied to the observed structure amplitudes (7.0–2.6 Å) in the latter stages of refinement to correct for the noticeable anisotropic fall-off in intensity of the data. This decreased the free R value by 3%–4% (the final anisotropic parameters with respect to the B-factor array are $B_{11} = B_{22} = 9.95$ Å^2, $B_{33} = -19.91$ Å^2, $B_{12} = 12.92$ Å^2).

The βD2–βA2 ard βH1–βI1 loops, which are located close to the interface between monomers 107A–108A and 185A–191A (and noncrystallographic symmetry-related regions 107B–108B, 186B–191B, and 189C–190C), as well as the final six residues at the C-terminus of PCNA 256A–261A (256B–261B, 256C–261C) and four at the N-terminus of the peptide, were omitted from the final model owing to poor electron density in those regions (A, B, and C refer to the three molecules in the asymmetric unit). Side chains were not modeled beyond C^β for the following amino acids: Asn-107C, Gln-108C, Glu-109A (109B, 109C), Asp-165C, Ser-186C, Asn-187C, Glu-191A (191B,191C), Glu-198A (198B), Arg-210B, Asp-232A(232B,232C), Ile-255A(255B,255C) of PCNA, and Arg-143A (Arg-143B, Arg-143C) of the peptide.

Refinement of a model containing 6,449 nonhydrogen atoms including 295 water molecules converged at values of 28.9 and 19.2 for the free R value and the working R value, respectively, for 22,893 reflections between 7.0 and 2.6 Å with $|F| \geq 2\sigma|F|$. The model has excellent geometry with a root-mean-square deviation in bond lengths of 0.008 Å and in angles 1.4°, and no Ramachandran outliers. The average B-factor for the protein model is 26.1 Å^2 and 33.9 Å^2 for water molecules. The root-mean-square deviation in B-factor is 2.9 Å^2 over all nonhydrogen atoms.

Acknowledgments

We thank David Lane, Jim Roberts, Bruce Stillman, and Emma Gibbs for insightful comments, Todd Yeates for suggesting the detwinning procedure, and David Lane for providing a 10 residue peptide for initial crystallization attempts. Critical assistance was provided by R. Suresh and T. S. R. Krishna during the early stages of this project. This work was partially supported by grants from the National Institutes of Health (GM 45547 to J. K., GM 38839 to M. O'D., and GM 38559 to J. H.). Support provided by Lonny Berman at Beamline X25 of the Brookhaven National Synchrotron Light Source is gratefully acknowledged.

Received August 15, 1996; revised September 9, 1996.

References

Almendral, J.M., Huebsch, D., Blundell, P.A., Macdonald-Brown, H., and Bravo, R. (1987). Cloning and sequence of the human nuclear protein cyclin: homology with DNA binding proteins. Proc. Natl. Acad. Sci. USA *84*, 1575–1579.

Bacon, D., and Anderson, W.F. (1988). A fast algorithm for rendering space-filling molecule pictures. J. Mol. Graph. *6*, 219–220.

Bauer, G.A., and Burgers, P.M. (1990). Molecular cloning, structure and expression of the yeast proliferating cell nuclear antigen gene. Nucl. Acids Res. *18*, 261–265.

Brünger, A.T. (1992). XPLOR Version 3.1: A System for X-Ray Crystallography and NMR (New Haven, Connecticut: Yale University).

Brünger, A.T., Krukowski, A., and Erickson, J.W. (1990). Slow-cooling protocols for crystallographic refinement by simulated annealing. Acta Cryst. *A46*, 585–593.

Chen, I.-T., Smith, M.L., O'Connor, P.M., and Fornace, J.A.J. (1995a). Direct interaction of Gadd45 with PCNA and evidence for competitive interaction of Gadd45 and $p21^{Waf1/Cip1}$ with PCNA. Oncogene *11*, 1931–1937.

Chen, J., Jackson, P.K., Kirschner, M.W., and Dutta, A. (1995b). Separate domains of p21 involved in the inhibition of Cdk kinase and PCNA. Nature *374*, 386–388.

Chen, J., Peters, R., Saha, P., Lee, P., Theodoras, A., Pagano, M., Wagner, G., and Dutta, A. (1996). A 39 amino acid fragment of the cell cycle regulator p21 is sufficient to bind PCNA and partially inhibit DNA replication in vivo. Nucl. Acids Res. *24*, 1727–1733.

El-Deiry, W.S., Tokino, T., Velculescu, V.E., Levy, D.B., Parsons, R., Trent, J.M., Lin, D., Mercer, W.E., Kinzler, K.W., and Vogelstein, B. (1993). Waf1, a potential mediator of p53 tumor suppression. Cell *75*, 817–825.

Flores-Rozas, H., Kelman, Z., Dean, F.B., Pan, Z.-Q., Harper, J.W., Elledge, S.J., O'Donnell, M., and Hurwitz, J. (1994). Cdk-interacting protein 1 directly binds with proliferating cell nuclear antigen and inhibits DNA replication catalyzed by the DNA polymerase δ holoenzyme. Proc. Natl. Acad. Sci. USA *91*, 8655–8659.

Fukuda, K., Morioka, H., Imajou, S., Ikeda, S., Ohtsuka, E., and Tsurimoto, T. (1995). Structure-function relationship of the eukaryotic DNA replication factor, proliferating cell nuclear antigen. J. Biol. Chem. *270*, 22527–22534.

Goubin, F., and Ducommun, B. (1995). Identification of binding domains on the $p21^{cip1}$ cyclin-dependent kinase inhibitor. Oncogene *10*, 2281–2287.

Gu, Y., Turck, C.W., and Morgan, D.O. (1993). Inhibition of CDK2 activity in vivo by a 20K regulatory subunit. Nature *366*, 707–710.

Hall, P.A., Kearsey, J.M., Coates, P.J., Norman, D.J., Warbrick, E., and Cox, L.S. (1995). Characterization of the interaction between PCNA and Gadd45. Oncogene *10*, 2427–2433.

Harper, J.W., Adami, G.R., Wei, N., Keyomarsi, K., and Elledge, S.J. (1993). The p21 Cdk-interacting protein Cip1 is a potent inhibitor of G1 cyclin-dependent kinases. Cell *75*, 805–816.

Jones, T.A., Zou, J.Y., Cowan, S.W., and Kjeldgaard, M. (1991). Improved methods for building protein models in electron density maps and the location of errors in these models. Acta Cryst. *A47*, 110–119.

Kelman, Z. (1996). Interactions between DNA polymerases and other cellular proteins. Ph.D. thesis, Cornell University Medical College, New York, New York.

Kelman, Z., and O'Donnell, M. (1995). Structural and functional similarities of prokaryotic and eukaryotic DNA polymerase sliding clamps. Nucl. Acids Res. *23*, 3613–3620.

Klewegt, G.J., and Jones, T.A. (1994). From the first map to final model. In Proceedings of the CCP4 Study Weekend, S. Bailey, R. Hubbard, and D. Waller, eds. (Daresbury, United Kingdom: Daresbury Laboratory), pp. 59–66.

Kong, X.-P., Onrust, R., O'Donnell, M., and Kuriyan, J. (1992). Three-dimensional structure of the β subunit of E. coli DNA polymerase III holoenzyme: a sliding DNA clamp. Cell *69*, 425–437.

Kraulis, P. (1991). MOLSCRIPT: a program to produce both detailed and schematic plots of protein structures. J. Appl. Cryst. *24*, 946–950.

Krishna, T.S.R., Kong, X.-P., Gary, S., Burgers, P., and Kuriyan, J. (1994). Crystal structure of the eukaryotic DNA polymerase processivity factor PCNA. Cell *79*, 1233–1243.

Lee, M.H., Reynisdottir, I., and Massagué, J. (1995). Cloning of p57KIP2, a cyclin-dependent kinase inhibitor with unique domain structure and tissue distribution. Genes Dev. *9*, 639–649.

Li, R., Hannon, G.J., Beach, D., and Stillman, B. (1996). Subcellular distribution of p21 and PCNA in normal and repair-deficient cells following DNA damage. Curr. Biol. *6*, 189–199.

Li, R., Waga, S., Hannon, G.J., Beach, D., and Stillman, B. (1994). Differential effects by the p21 CDK inhibitor on PCNA–dependent DNA replication and repair. Nature *371*, 534–537.

Luo, Y., Hurwitz, J., and Massagué, J. (1995). Cell-cycle inhibition by independent CDK and PCNA binding domains in $p21^{cip1}$. Nature *375*, 159–161.

Matsuoka, S., Yamaguchi, M., and Matsukage, A. (1994). D-type cyclin-binding regions of proliferating cell nuclear antigen. J. Biol. Chem. *269*, 11030–11036.

Nakanishi, M., Robetoyre, R.S., Pereira-Smith, O.M., and Smith, J.R. (1995). The C-terminal region of $p21^{SDI1/WAF1/CIP1}$ is involved in proliferating cell nuclear antigen binding but does not appear to be required for growth inhibition. J. Biol. Chem. *270*, 17060–17063.

Nicholls, A., Sharp, K.A., and Honig, B. (1991). Protein folding and association: insights from the interfacial and thermodynamic properties of hydrocarbons. Proteins: Struct. Funct. Genet. *11*, 281–296.

Nichols, A.F., and Sancar, A. (1992). Purification of PCNA as a nucleotide excision repair protein. Nucl. Acids Res. *20*, 2441–2446.

Noda, A., Ning, Y., Venable, S.F., Pereira Smith, O.M., and Smith, J.R. (1994). Cloning of senescent cell-derived inhibitors of DNA synthesis using an expression screen. Exp. Cell Res. *211*, 90–98.

Pan, Z.-Q., Reardon, J.T., Li, L., Flores-Rozas, H., Legerski, R., Sancar, A., and Hurwitz, J. (1995). Inhibition of nucleotide excision repair by the cyclin-dependent kinase inhibitor p21. J. Biol. Chem. *270*, 22008–22016.

Peter, M., and Herskowitz, I. (1994). Joining the complex: cyclin-dependent inhibitory proteins and the cell cycle. Cell *79*, 181–184.

Podust, V.N., Podust, L.M., Goubin, F., Ducommun, B., and Hübscher, U. (1995). Mechanism of inhibition of proliferating cell nuclear antigen–dependent DNA synthesis by the cyclin-dependent kinase inhibitor p21. Biochemistry *34*, 8869–8875.

Polyak, K., Lee, M.-H., Erdjument-Bromage, H., Koff, A., Roberts, J.M., Tempst, P., and Massagué, J. (1994). Cloning of $p27^{Kip1}$, a cyclin-dependent kinase inhibitor and a potential mediator of extracellular antimitogenic signals. Cell *78*, 59–66.

Redinbo, M.R., and Yeates, T.O. (1993). Structure determination of plastocynanin from a specimen with a hemihedral twinning fraction of one-half. Acta Cryst. *D49*, 375–380.

Robbins, J., Dilworth, S.M., Laskey, R.A., and Dingwall, C. (1991). Two interdependent basic domains in nucleoplasmin nuclear targeting sequence: indentification of a class of bipartite nuclear targeting sequence. Cell *64*, 616–623.

Roos, G., Jiang, Y., Landberg, G., Nielsen, N.H., Zhang, P., and Lee, M.Y.W.T. (1996). Determination of the epitope of an inhibitory antibody to proliferating cell nuclear antigen. Exp. Cell Res., in press.

Russo, A.A., Jeffrey, P.D., Patten, A.K., Massagué, J., and Pavletich, N.P. (1996). Crystal structure of the $p27^{Kip1}$ cyclin-dependent–kinase inhibitor bound to the cyclin A–Cdk2 complex. Nature *382*, 325–331.

Shivji, M.K.K., Kenny, M.K., and Wood, R.D. (1992). Proliferating cell nuclear antigen is required for DNA excision repair. Cell *69*, 367–374.

Shivji, M.K.K., Grey, S.J., Strausfeld, U.P., Wood, R.D., and Blow, J.J. (1994). Cip1 inhibits DNA replication but not PCNA–dependent nucleotide excision-repair. Curr. Biol. *4*, 1062–1068.

Smith, M.L., Chen, I.-T., Zhan, Q., Bae, I., Chen, C.-Y., Gilmer, T.M., Kastan, M.B., O'Connor, P.M., and Fornace, A.J., Jr. (1994). Interaction of the p53-regulated protein Gadd45 with proliferating cell nuclear antigen. Science *266*, 1376–1380.

Su, J.-Y., Rempel, R.E., Erikson, E., and Maller, J.L. (1995). Cloning and characterization of the Xenopus cyclin-dependent kinase inhibitor $p27^{xic1}$. Proc. Natl. Acad. Sci. USA *92*, 10187–10191.

Waga, S., Hannon, G.J., Beach, D., and Stillman, B. (1994). The p21 inhibitor of cyclin-dependent kinases controls DNA replication by interaction with PCNA. Nature *369*, 574–578.

Waldman, T., Lengauer, C., Kinzler, K.W., and Vogelstein, B. (1996). Uncoupling of S phase and mitosis by anticancer agents in cells lacking p21. Nature *381*, 713–716.

Warbrick, E., Lane, D.P., Glover, D.M., and Cox, L.S. (1995). A small peptide inhibitor of DNA replication defines the site of interaction between the cyclin-dependent kinase inhibitor p21waf1 and the proliferating cell nuclear antigen. Curr. Biol. *5*, 275–282.

Xiong, Y., Zhang, H., and Beach, D. (1993). D type cyclins associate with multiple protein kinases and the DNA replication and repair factor PCNA. Cell *71*, 505–514.